ACS EARTH AND SPACE CHEMISTRY

Article

Cite This: ACS Earth Space Chem. 2019, 3, 1631−1639

http://pubs.acs.org/journal/aesccq

Magmatic-Hydrothermal Origin of Mercury in Carlin-style and Epithermal Gold Deposits in China: Evidence from Mercury Stable Isotopes

Runsheng Yin,*[,†] Changzhou Deng,[‡] Bernd Lehmann,[§] Guangyi Sun,[#] Ryan F. Lepak,[∇] James P. Hurley,[∇] Chenghai Zhao,[†] Guiwen Xu,[†] Qinping Tan,[†] Zhuojun Xie,[†] and Ruizhong Hu[†]

[†]State Key Laboratory of Ore Deposit Geochemistry, Institute of Geochemistry, Chinese Academy of Sciences, Guiyang 550081, China

[‡]College of Earth Sciences, Jilin University, Changchun 130061, China

[§]Mineral Resources, Technical University of Clausthal, 38678 Clausthal-Zellerfeld, Germany

[#]State Key Laboratory of Environmental Geochemistry, Institute of Geochemistry, Chinese Academy of Sciences, Guiyang 550081, China

[∇]Environmental Chemistry and Technology Program, University of Wisconsin—Madison, Madison, Wisconsin 53706, United States

Supporting Information

ABSTRACT: Carlin-style (sediment-hosted, "invisible" gold) and epithermal gold deposits are commonly enriched in mercury (Hg), but the source of this metal is not well-known. In the world, the association of Hg with gold is often related to magmatism; however, it is still unclear whether magmatism serves as a direct Hg source in gold deposits or only an energy source that drives hydrothermal circulation and leaches Hg from sedimentary country rocks. Here, we use Hg stable isotopes to directly indicate the source of Hg in a major Carlin-style gold deposit (Shuiyindong) and two small epithermal gold deposits (Xianfeng and Sishanlinchang) in China. In the three deposits, mineralized rocks (Au > 0.10 μg/g) are elevated in Hg levels by 1 to 3 orders of magnitude, compared to barren rocks (Au < 0.05 μg/g). The majority of the mineralized rocks in all three deposits show quite narrow ranges of δ^{202}Hg (−1 to 0.5‰) and Δ^{199}Hg (−0.1 to 0.1‰). The absence of significant mass-independent fractionation signals of Hg in mineralized rocks (Δ^{199}Hg ≈ 0) is consistent with magmatic rocks, implying Hg was either leached from already crystalline magmatic rocks or directly mass transferred from a silicate magma via magmatic-hydrothermal fluid. Our reconnaissance study thus indicates a dominant origin of magmatic Hg for the three gold deposits.

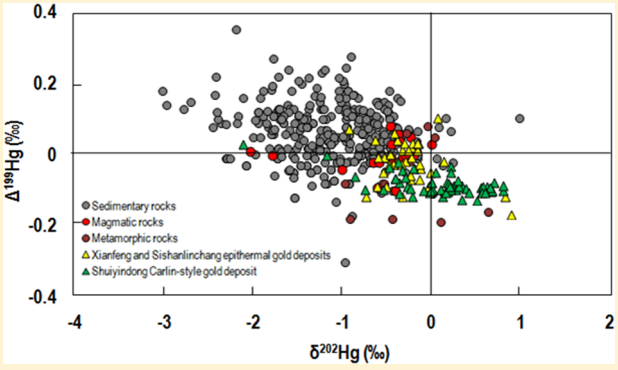

KEYWORDS: *Mercury isotopes, Isotope fractionation, Source tracing, Gold deposits, Magmatic-hydrothermal fluid model*

INTRODUCTION

Gold (Au) deposits occur in a large range of geodynamic settings and are hosted in a variety of rock types. The broad pressure−temperature spectrum of their formation is used for the traditional classification into near-surface epithermal gold deposits and deeper and hotter mesothermal orogenic gold deposits.[1,2] Another important group of gold deposits, known as Carlin-type, has disseminated mineralization of submicron-sized gold in silicified and partly decarbonated carbonaceous rocks.[3,4] All these above-mentioned gold deposits have a common enrichment of mercury (Hg).[5] Although Hg has long been used as a pathfinder for the geochemical exploration for gold deposits,[6] its origin is not well understood. The association of Hg with Au is often related to magmatism and thermal-spring activity, as we see in many areas of the world today (e.g., New Zealand, Japan, and Russia), and this association is seen throughout geologic time. In the world, gold deposits often show a close spatial and/or temporal association with magmatic rocks. It is, however, still unclear whether magmatism serves as a source of Hg in these gold deposits or only as an energy source that drives hydrothermal circulation and leaches Hg from sedimentary country rocks.

Mercury isotopes are useful tracers on the origin of Hg in hydrothermal deposits.[7−10] Mercury has seven natural isotopes (^{196}Hg, ^{198}Hg, ^{199}Hg, ^{200}Hg, ^{201}Hg, ^{202}Hg, and ^{204}Hg). Mass-

Received: April 27, 2019
Revised: June 9, 2019
Accepted: June 11, 2019
Published: June 11, 2019

DOI: 10.1021/acsearthspacechem.9b00111
ACS Earth Space Chem. 2019, 3, 1631−1639

dependent fractionation (MDF, denoted here as δ^{202}Hg) of Hg isotopes can occur during almost all physical, chemical, and biological processes. Hg isotopes also undergo mass-independent fractionation (MIF, denoted as Δ^{199}Hg, Δ^{200}Hg, or Δ^{201}Hg) during specific processes.[11−14] The MIF signature of Hg observed in natural samples is believed to be mainly caused by Hg photochemical reactions.[15−17] In hydrothermal processes, the release of Hg from source rocks seems to cause little to no Hg-MDF (<±0.5‰ in δ^{202}Hg),[8,11] but redox reactions and boiling of hydrothermal fluids can result in significant Hg-MDF (up to 4‰ in δ^{202}Hg).[7] Hydrothermal processes will not cause significant Hg-MIF,[7,8] which allows Hg-MIF to act as a direct source tracer of Hg in hydrothermal deposits. Distinct Hg-MIF signatures have been observed for different source rocks. For instance, sedimentary rocks showed large variations of Δ^{199}Hg (−0.3 to 0.4‰), whereas small or no Hg-MIF was observed in metamorphic rocks (−0.2 to 0.1‰) and magmatic rocks (−0.1 to 0.1‰).[8,10,18−25] Pronounced Hg-MIF signals (Δ^{199}Hg: −0.30 to 0.24‰) have been observed in some Pb−Zn hydrothermal deposits and have been interpreted as the inheritance of primary surficial signatures via sedimentation and hydrothermal leaching.[9,10,26]

China has become the largest gold-producing country over the past few years.[27] A large number of epithermal and Carlin-style (or Carlin-like) gold deposits were discovered in NE China and SW China, respectively (Figure S1-A). There has been much controversy concerning the fluid sources in the two areas, with magmatic, metamorphic, or meteoric fluids all suggested by various authors.[28−31] In particular, the source of Hg in these gold deposits remains a mystery. Using Hg isotopes as a direct source tracer, the present study investigated the isotopic variation of Hg in two small epithermal gold deposits (Xianfeng and Sishanlichang) in NE China and the major Carlin-style gold deposit of Shuiyindong in SW China. By comparing the isotopic difference of Hg in mineralized rocks and spatially associated potential source rocks from the three gold deposits, this study aimed (1) to discern whether Hg sources are different between epithermal and Carlin-style gold deposits and (2) to understand potential Hg isotope fractionation processes during the formation of these gold deposits.

EXPERIMENTAL SECTION

Regional Geology. The Xianfeng and Sishanlinchang gold deposits are located in the easternmost part of the Central Asian Orogenic Belt (CAOB) where it overlaps with the accretionary orogen of the Western Pacific porphyry-epithermal gold−copper metallogenic belt.[32] The regional geology is characterized by the Jiamusi-Xingkai and the Wandashan massifs or terranes (Figure S1-B) that amalgamated during the late Mesozoic.[33]

The Jiamusi-Xingkai Massif consists of the Heilongjiang Complex, the Mashan Complex, and Paleozoic granitic intrusions.[34] The Heilongjiang complex is predominately composed of alternating pelitic schists and blue schists with intercalations of thin layers of quartzites and marbles and of ultramafic bodies.[35] The Mashan Complex consists of upper amphibolite to granulite facies metamorphic rocks, which were thought to be the basement of the Jiamusi Massif.[35] SHRIMP U/Pb dating of metamorphic zircons suggests that the metamorphism of the Mashan Complex took place at ca. 500 Ma.[36] Two stages of Paleozoic granitoids have been identified, the ca. 520-Ma-year-old deformed and metamorphosed granitoids and the ca. 260-Ma-year-old weakly or undeformed granitoids.[37] The igneous and metamorphic basement is intruded and overlain by Early Jurassic-Early Cretaceous volcanic plutonic rocks and Cenozoic basalts.[35] A number of NE trending faults control the location of several epithermal gold deposits (e.g., Sishanlinchang, Jinchang, and Tuanjiegou).

The Wandashan Massif consists of a metamorphic mélange in its eastern part.[38] The mélange consists of upper green schist facies mica-schist, marble, and meta-mafic and ultramafic igneous rocks. The western part of the Wandashan Massif is composed of accreted mid-Triassic to mid-Jurassic radiolarian chert and ultramafic−mafic rocks, and Late Jurassic to Early Cretaceous trench-slope terrestrial-sourced clastic rocks.[38] Numerous epithermal gold deposits (e.g., Xianfeng, Sipingshan, and Yuejinshan) are related to Early Cretaceous volcano plutonic activity.

Carlin-style gold deposits in China mainly occur in the Youjiang Basin, the Yunnan-Guizhou-Guangxi "golden triangle" (Figure S1C), with a total resource of >700 t Au.[39] The Basin is at the juncture of the westward extension of the Cathaysia Foldbelt and the southwestern margin of the South China Block and was formed during the opening of the Paleo-Tethys Ocean in the Devonian followed by deposition of a carbonate platform and shallow-water facies sediments in the Late Paleozoic and deep-water sediments (siltstone and sandstone turbidites) in the Middle Triassic.[40] Granite plutons and felsic dikes, with ages ranging from 96 to 80 Ma, are present at the fringes of the Youjiang Basin and nearby regions,[39,40] and sparse igneous rocks are mainly alkaline ultramafic rocks that intruded Permian to Triassic units.[41] Su et al.[42] recently observed aeromagnetic anomalies throughout the Youjiang Basin, suggesting broad hidden intrusions under this basin. The Youjiang Basin hosts a large number of Carlin-type gold deposits (e.g., Shuiyindong, Zimudang, and Yata), and their distribution is controlled by NW- and NE- trending regional folds and faults.[29,42]

Local Geology. The Xianfeng deposit, located in the western part of the Wadashan Massif (Figure S1B), is contained in volcanic rocks that mainly consist of 116 Ma rhyolitic tuffs, rhyolites, dacites, and hydrothermal breccias (Figure S2A). Ore barren igneous rocks, including 128 Ma granodiorite and 106 Ma diorite porphyry, were distributed mainly in the northwestern part of the deposit.[43] It is part of a ∼117 Ma epithermal system, with ore formation temperatures of 105−277 °C and low salinity of 0.7 to 5.4 wt % $NaCl_{eqv}$.[43] Numerous brecciated, veined, and lenticular orebodies have been identified along an EW-trending fracture zone. The gold resource in Xianfeng is confidential; however, the largest orebody (120 m × 115 m × 50 m in size) is reported to have a grade of 4.9 g/t Au in average.[43] The mineralogy and alteration characteristics of the Xianfeng deposit have been reported previously.[44,45] The ore textures are typical of open-space filling, with quartz and calcite banding, crustification, and blade textures. Pyrite and hematite and minor chalcopyrite and magnetite are the ore minerals. Pyrite is the most abundant sulfide and the primary gold-bearing mineral. Native gold (>1 μm) occurs in pyrite or along quartz crystal boundaries. Gangue minerals include quartz, calcite, chalcedony, and adularia. Hydrothermal alteration mainly includes silicification, carbonatization, sericitization, and kaolinization. Mineralogy and alteration classify this system as adularia-sericite type with

DOI: 10.1021/acsearthspacechem.9b00111
ACS Earth Space Chem. 2019, 3, 1631−1639

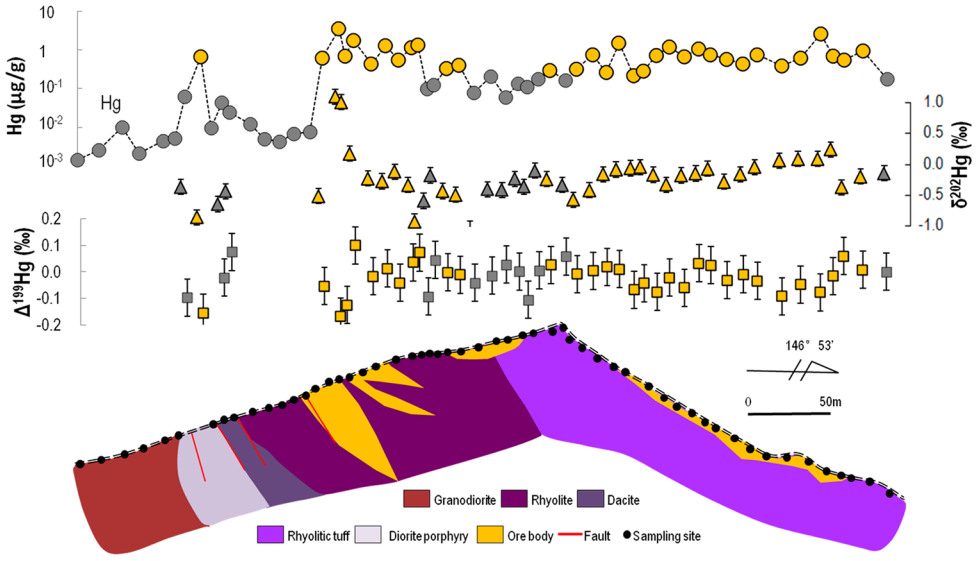

Figure 1. Hg concentrations and isotopic compositions of bulk rock samples from the Xianfeng epithermal gold deposit. Symbols in yellow represent samples with gold mineralization (Au > 0.10 μg/g), and symbols in gray represent barren samples (Au < 0.05 μg/g). Note: the *Y*-axis for Hg concentration is on a log-scale.

a low to intermediate sulfidation state. According to the mineral assemblages and crosscutting relations of veins, three individual stages of mineralization have been identified: an early gray-white quartz vein stage in volcanic rocks, a gray and black chalcedony stage with fine-grained pyrite, and a late white quartz stage with carbonatization.[45]

The Sishanlinchang deposit is hosted in the contact zone between the Cretaceous diorite porphyry and the Proterozoic Yanwangdian Formation (Figure S2B) at the eastern part of the Jiamusi-Xingkai massif (Figure S1B). The Yanwangdian Formation is composed of green schist facies carbonaceous quartz schist. Igneous rocks, including granite porphyry, granodiorite porphyry, and diorite porphyry, occur as stocks and dikes scattered within the Yanwangdian Formation. The ore bodies occur as disseminations, veinlets, stockworks, and in brecciated vein structures.[46] Ore formation temperatures are 150 to 310 °C and low salinity of 4 to 13 wt % $NaCl_{eqv}$.[46] The gold resource is >10 t Au. Molybdenite Re−Os dating (111.1−111.4 Ma) suggests that the deposit formed in the late Early Cretaceous.[47] The mineralogy and alteration characteristics of Sishanlinchang were previously reported.[46] Briefly, the sulfide minerals in the Sishanlinchang deposit consist of pyrite and arsenopyrite and minor galena, sphalerite, molybdenite, chalcopyrite, and bornite. Native gold (0.07 to 0.3 mm in diameter) occurs in pyrite and arsenopyrite. The gangue minerals consist of quartz, feldspar, chlorite, sericite, and carbonate. Silicification, sericitization, epidotization, chloritization, kaolinization, and carbonatization are generally recognized around the ore bodies. Ore mineralogy and alteration features characterize the system as epithermal and in an intermediate sulfidation state.

The Shuiyindong deposit, located in the Youjiang Basin (Figure S1C), is one of the largest Carlin-type gold deposits in China. This deposit contains 263 tonnes of Au at an average grade of 5 g/t Au.[41] The ore-forming fluid of this deposit was of low temperature (190−278 °C) and low salinity (4.2 to 6.9 wt % $NaCl_{eqv}$).[42] Calcite Sm−Nd dating by Su et al.[48] suggests that this deposit formed at 134−136 Ma. The major exposed sedimentary bedrocks at the Shuiyindong deposit are Middle and Upper Permian and Lower Triassic strata, which were folded into the E−W trending Huijiabao anticline where orebodies occur near its axial part (Figure S2C). Orebodies are predominantly disseminated in limestone and calcareous siltstone of the Upper Permian Longtan Formation and at the unconformity between the Moukou and Longtan Formations.[28,48] The mineralogy and alteration characteristics of the Shuiyindong deposit were previously described.[48] Wall-rock alteration is mainly silicification, dolomitization, and argillic alteration, with the introduction of much arsenian pyrite, arsenopyrite, realgar, and fluorite. Silicification, dolomitization, and pyritization (pyrite + arsenopyrite) have a close relation to gold mineralization. Ore minerals mainly consist of pyrite, arsenopyrite, and marcasite, and small amounts of orpiment, realgar, and stibnite. Gold predominantly occurs in arsenian pyrite.[49] Quartz, calcite, dolomite, sericite, illite, and kaolinite are the major gangue minerals.[42]

Sampling and Analytical Methods. Rock samples were collected from an NW−SE transect at Xianfeng (Figure S2A), two drill cores at Sishanlinchang (Figure S2B), and three drill cores at Shuiyindong (Figure S2C). The samples were precleaned with deionized water, dried at room temperature, crushed and ground (agate shatter box), and sieved to subminus 150 mesh before chemical analysis. Bulk gold concentrations of rock samples were measured using the commercial fire assay technique with gravimetric finish (Code Au-GRA22) by ALS-Chemex Co. Ltd., Guangzhou, China (detection limit: 0.05 μg/g). Bulk Hg concentrations of the samples were determined using a Lumex RA 915+ Hg analyzer (detection limit: 0.5 ng/g) at the Institute of Geochemistry, Chinese Academy of Sciences. Analytical accuracy was evaluated by measuring standard reference materials (SRMs) such as GSR-1 (granite, n = 3), NIST SRM 2711 (Montana Soil II, n = 3), and MESS-2 (marine sediment, n = 3). Accuracy of Hg for all SRMs is within 88 to 114% of the reported values.

Hg isotopes were analyzed by a Neptune Plus multiple collector inductively coupled plasma mass spectrometer at the State Laboratory of Hygiene, University of Wisconsin—

DOI: 10.1021/acsearthspacechem.9b00111
ACS Earth Space Chem. 2019, 3, 1631−1639

Madison.[50] For samples with Hg concentrations ≥25 ng/g, 0.2 g of sample powder was digested (95 °C, 6 h) in a 2 mL acid mixture (HCl/HNO_3 = 3, v/v). Samples with Hg concentrations < 25 ng/g were not prepared for Hg isotope analysis. NIST SRM 2711 (n = 9) and MESS-2 (n = 9) were similarly prepared. The digests were diluted to 0.5 ng/mL Hg with an acid concentration of 10 to 20%. Hg concentrations and acid matrixes of NIST SRM 3133 and UM-Almadén standard solutions were similar to those in the sample solutions. δ^{202}Hg, Δ^{199}Hg, Δ^{200}Hg, and Δ^{201}Hg were calculated relative to NIST SRM 3133, following the protocol by Blum and Bergquist.[51] Our results of UM-Almadén (δ^{202}Hg: −0.50 ± 0.11‰; Δ^{199}Hg: −0.02 ± 0.06‰; 2SD, n = 23), NIST SRM 2711 (δ^{202}Hg: −0.19 ± 0.11‰; Δ^{199}Hg: −0.21 ± 0.04‰; 2SD, n = 3), and MESS-2 (δ^{202}Hg: −1.84 ± 0.11‰; Δ^{199}Hg: 0.03 ± 0.03‰; 2SD, n = 3) are consistent with reported values.[50−52] The larger values of standard deviation (2SD) for either UM-Almadén or SRMs are used to reflect analytical uncertainties.

RESULTS

Au and Hg Concentrations. Variations of bulk Au and Hg concentrations (Tables S1−S3) in rock samples from the three deposits are illustrated in Figures 1−3. Gold concentrations ranged from <0.05 to 5.20, < 0.05 to 2.6, and <0.05 to 22.92 μg/g in the Xianfeng, Sishanlinchang, and Shuiyindong deposits, respectively. The samples were classified into two groups according to Au concentration for further statistical analysis, i.e., rocks with Au > 0.10 μg/g (denoted as $rocks_{Au>0.10}$) for mineralized samples and rocks with Au < 0.05 μg/g (denoted as $rocks_{Au<0.05}$) for barren samples. The $rocks_{Au>0.10}$ samples in the Xianfeng, Sishanlinchang, and Shuiyindong deposits have geometric means of 0.33 μg/g Au (n = 33), 0.67 μg/g Au (n = 8), and 0.51 μg/g Au (n = 76), respectively.

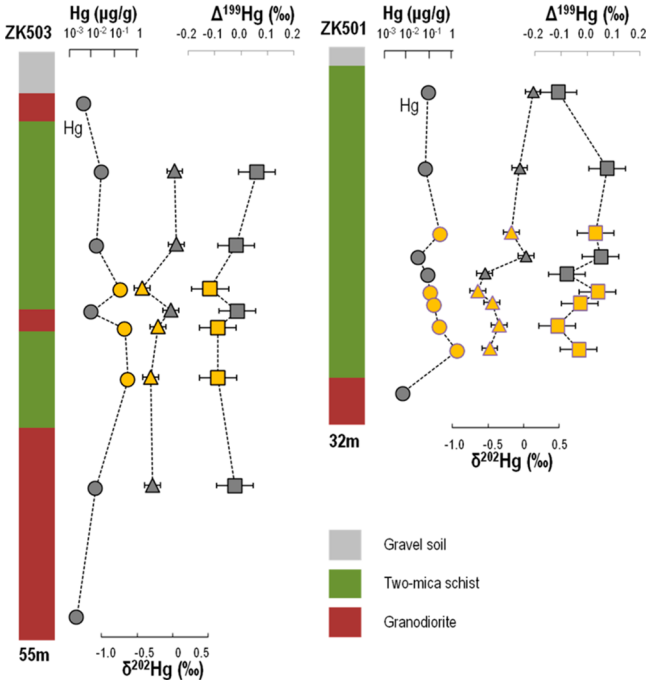

Figure 2. Hg concentrations and isotopic compositions of bulk rock samples from the Sishanlichang epithermal gold deposit. Symbols in yellow represent samples with gold mineralization (Au > 0.10 μg/g), and symbols in gray represent barren samples (Au < 0.05 μg/g). Note: the X-axis for Hg concentration is on a log-scale.

In the three deposits, mineralized $rocks_{Au>0.10}$ are elevated in Hg levels by 1 to 3 orders of magnitude when compared to barren $rocks_{Au<0.05}$ (Figures 1−3). Some of the barren $rocks_{Au<0.05}$ peripheral to the mineralized $rocks_{Au>0.10}$ also show extremely high Hg levels, which reflects the large geochemical halos of Hg around the deposits. Hg concentrations of each deposit follow a log-normal distribution (Figure 4); therefore, geometric mean values are reported. In the Xianfeng deposit, $rocks_{Au>0.10}$ and $rocks_{Au<0.05}$ have geometric mean concentrations of 0.68 μg/g Hg (n = 33) and 0.02 μg/g Hg (n = 25), respectively. In the Sishanlinchang deposit, $rocks_{Au>0.10}$ have geometric means of 0.28 μg/g Hg (n = 8), much higher than $rocks_{Au<0.05}$ such as schist (0.02 μg/g, n = 8) and granodiorite (0.01 μg/g, n = 3). In the Shuiyindong deposit, the geometric mean of $rocks_{Au>0.10}$ was 2.76 μg/g Hg (n = 76); these rocks were located at the Upper Permian Longtan Formation. Barren $rocks_{Au<0.05}$ in the Upper Permian Longtan Formation (mainly altered limestone and calcareous siltstone) also have elevated Hg concentrations (0.43 μg/g, n = 98); however, much lower Hg concentrations (0.01 μg/g, n = 20) were observed for barren $rocks_{Au<0.05}$ in other strata (mainly nonaltered limestone).

Hg Isotopic Composition. Variations of bulk Hg isotopic compositions (Tables S1−S3) in rock samples from the three deposits are illustrated in Figures 1,−3. According to the Shapiro-wilk test (p < 0.1), the δ^{202}Hg and Δ^{199}Hg follow a normal distribution; therefore, arithmetic mean values are reported. Similar Hg isotopic signals were observed for $rocks_{Au>0.10}$ and $rocks_{Au<0.05}$ from both the Xianfeng and Sishanlinchang deposits (Figure 4). In the Xianfeng deposit, $rocks_{Au>0.10}$ have mean δ^{202}Hg and Δ^{199}Hg values of −0.23 ± 0.72‰ and −0.02 ± 0.12‰, respectively (2 SD, n = 33), which are comparable (p > 0.05 for both, t test) to that of $rocks_{Au<0.05}$ (δ^{202}Hg: −0.46 ± 0.44 ‰; Δ^{199}Hg: −0.02 ± 0.12 ‰; 2 SD, n = 13). In the Sishanlinchang deposit, $rocks_{Au>0.10}$ (δ^{202}Hg: −0.49 ± 0.36 ‰; Δ^{199}Hg: −0.05 ± 0.11 ‰, 2 SD, n = 8) showed no statistic difference (p > 0.05, ANOVA) in δ^{202}Hg and Δ^{199}Hg values to $rocks_{Au<0.05}$, i.e., granodiorite (δ^{202}Hg: −0.47 ± 0.36 ‰; Δ^{199}Hg: −0.03 ± 0.02 ‰, 2 SD, n = 2) and schist (δ^{202}Hg: −0.15 ± 0.54 ‰; Δ^{199}Hg: 0.00 ± 0.18 ‰, 2 SD, n = 5).

In the Shuiyindong deposit, however, a large difference in Hg isotopic composition can be observed between $rocks_{Au>0.10}$ and $rocks_{Au<0.05}$ (Figure 4). The mineralized $rocks_{Au>0.10}$ in the Longtan Formation have mean δ^{202}Hg of 0.05 ± 1.06 ‰ (2 SD, n = 56), slightly higher (p < 0.05, t test) than that of barren $rocks_{Au<0.05}$ in the Longtan Formation (−0.73 ± 1.98 ‰, 2 SD, n = 51) but much higher (p < 0.01, t test) than that of barren $rocks_{Au<0.05}$ in other strata (−1.38 ± 1.12 ‰, 2 SD, n = 62). Slightly negative or no Hg-MIF was observed for mineralized $rocks_{Au>0.10}$ (Δ^{199}Hg: −0.08 ± 0.06 ‰, 2 SD, n = 56) and barren $rocks_{Au<0.05}$ (Δ^{199}Hg: −0.06 ± 0.10 ‰, 2 SD, n = 51) in the Longtan Formation, whereas barren $rocks_{Au<0.05}$ from other strata showed slightly positive to no Hg-MIF (Δ^{199}Hg: 0.06 ± 0.10 ‰, 2 SD, n = 62). In a recent study,[53] gold-bearing pyrites from the Shuiyindong deposit showed consistent δ^{202}Hg (−0.33 to 0.1‰; −0.12 ± 0.31 ‰; 2SD, n = 5) and Δ^{199}Hg (−0.06 to 0.03‰; −0.04 ± 0.08 ‰; 2SD, n = 5) values with $rocks_{Au>0.10}$ samples.

DOI: 10.1021/acsearthspacechem.9b00111
ACS Earth Space Chem. 2019, 3, 1631−1639

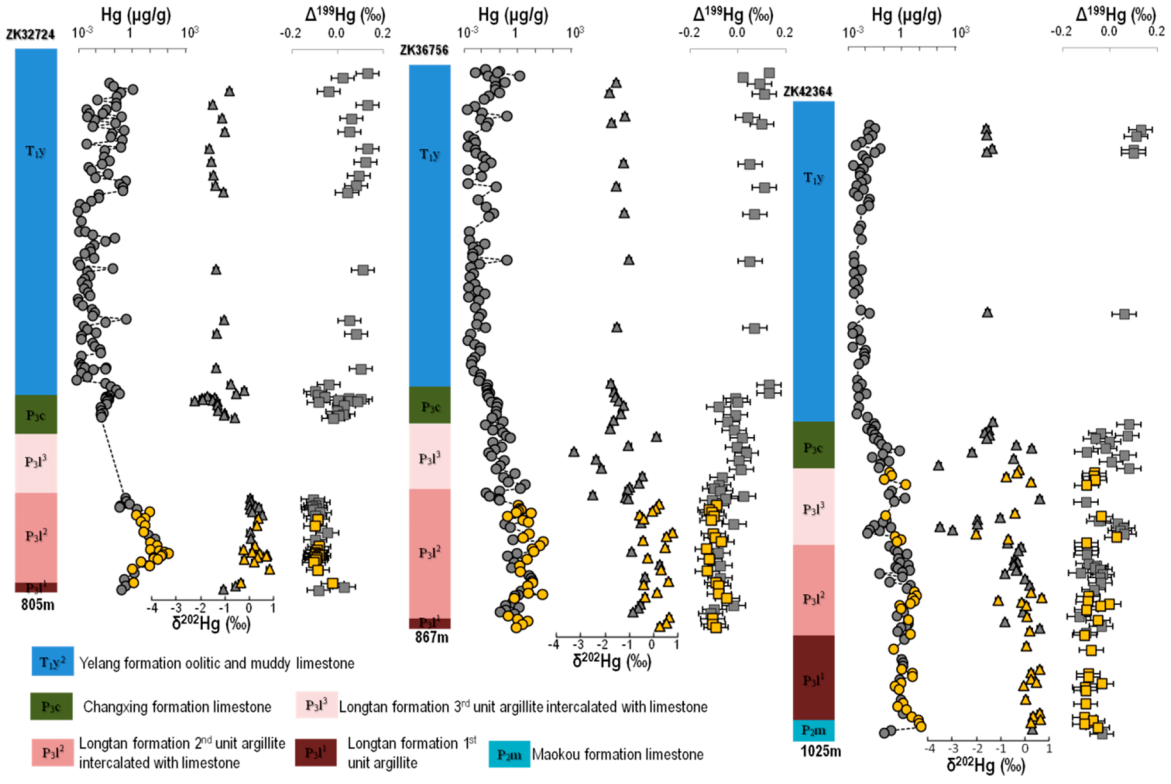

Figure 3. Hg concentrations and isotopic compositions of bulk rock samples from the Shuiyindong Carlin-type gold deposit. Symbols in yellow represent samples with gold mineralization (Au > 0.10 μg/g), and symbols in gray represent barren samples (Au < 0.05 μg/g). Note: the *X*-axis for Hg concentration is on a log-scale.

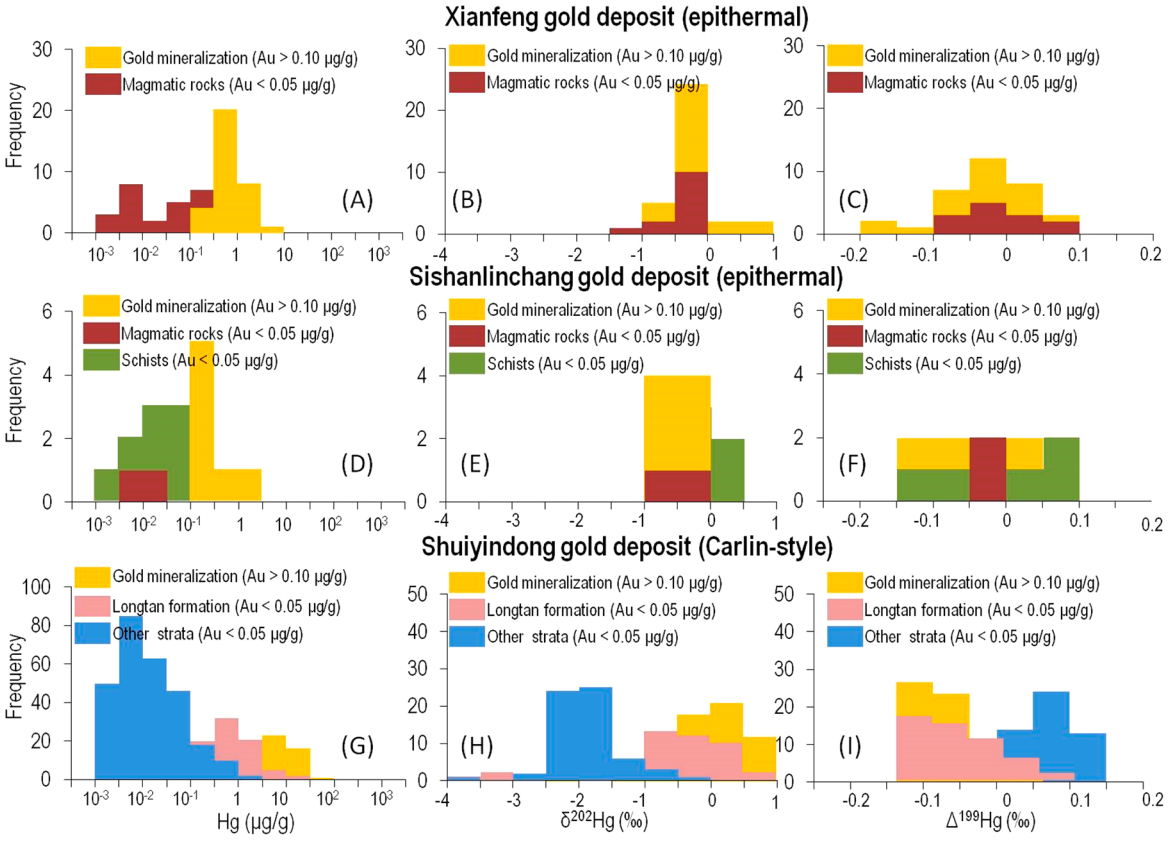

Figure 4. Histograms of Hg concentrations (A, D, G), δ^{202}Hg (B, E, H), and Δ^{199}Hg (C, F, I) for the Xianfeng and Sishanlinchang epithermal gold deposits and the Shuiyindong Carlin-type gold deposit. Note: the *X*-axis for Hg concentration is on a log-scale.

DOI: 10.1021/acsearthspacechem.9b00111
ACS Earth Space Chem. 2019, 3, 1631−1639

DISCUSSION

Relationship between Au, Hg, and Magmatism. The enrichment of Hg in mineralized rocks$_{Au>0.10}$ from the Xianfeng and Sishanlinchang gold deposits is consistent with general features of epithermal gold deposits (see reviews by Zhu et al.[54] and Saunders et al.[55]), which has been well-known since the definition of epithermal ore deposits by Waldemar Lindgren in the 1920s.[1] Volcanic-arc related magmatism is believed to play a critical role in the formation of epithermal gold deposits.[56] The Xianfeng and Sishanlinchang deposits formed at about 117 Ma according to Wang[43] and 111 Ma according to Huang et al.,[47] respectively, in accord with the Early Cretaceous magmatism caused by the Cretaceous plate subduction in the west Pacific.[57] The Xianfeng gold deposit is believed to be of magmatic-hydrothermal origin as it is hosted in hydrothermal breccias of the Early Cretaceous rhyolite. The Sishanlinchang deposit also has a close relationship to magmatism as it is hosted in the contact zone between diorite porphyry and the two-mica schist of the Proterozoic Yanwangdian Formation (Figure S2B). The δ^{34}S values of ores in the Sishanlinchang deposit (−1.8 to 5‰, according to Huang et al.[47]) are within the range of that reported for most igneous rocks (0 ± 5‰, according to Ohmoto,[58] and Rye and Ohmoto[59]), suggesting that the majority of sulfur came from igneous rocks. The low Hg levels in barren rocks$_{Au<0.05}$ from the Xianfeng and Sishanlinchang deposits are consistent with previous studies that show low Hg abundances in nonaltered magmatic and metamorphic rocks.[8−10] Mercury and other volatile components (e.g., sulfur) tend to escape at elevated temperatures from silicate magma to magmatic-hydrothermal fluid phase due to their tendency to vaporize and to form aqueous sulfide complexes.[60] It is expected that the high-temperature magmatic processes (e.g., partial melting) should cause limited isotope fractionation of Hg.[61]

In the Carlin-style Shuiyindong deposit, mineralized rocks$_{Au>0.10}$ and barren rocks$_{Au<0.05}$ from the Upper Permian Longtan Formation (mainly altered limestone and calcareous siltstone) have Hg levels that are 2 to 3 orders of magnitude higher than in other strata (mainly unaltered limestone) suggesting a broad geochemical halo of Hg much broader than the Au halo. The enrichment of Hg, the low temperature of ore formation (190−278 °C), and the low salinities (4.2 to 6.9 wt % NaCl$_{eqv}$) of the Shuiyindong deposit[42] show similarities to the Xianfeng and Sishanlinchang deposits that have a close relation with magmatism. The enrichment of Hg in the Shuiyindong deposit may also favor a magmatic-hydrothermal model. A recent study by Xie et al.[39] demonstrated that pyrite of the gold ore stage from the Shuiyindong deposit has a small variation of δ^{34}S (−3.3 to 2.5‰) consistent with previous results on igneous rocks (0 ± 5‰).[58,59] Identical to the Carlin district, USA, the Youjiang Basin has no major exposures of igneous rocks. There are, however, many small outcrops of diabase, felsic, and ultramafic dikes that follow the same NW- and NE-trending folds and faults as the gold mineralization. Su et al.[42] also observed broad aeromagnetic anomalies in the Youjiang Basin (more details can be found in Figure S3) suggesting broad hidden intrusions under this basin. Xie et al.[39] also identified a narrow range of δ^{34}S values (−5 to 5‰) for ore-related sulfide minerals from major Carlin-type gold deposits in the Youjiang Basin, which favors a magmatic-hydrothermal model of these deposits.

Consistent Hg Isotopic Signature in Gold Deposits. As shown in Figure 4, a consistent Hg isotopic signature was observed for rock$_{Au>0.10}$ samples from the three deposits. The isotopic signatures of rocks$_{Au>0.10}$ were overlapped with that of magmatic and metamorphic rocks. As summarized in Figure 5,

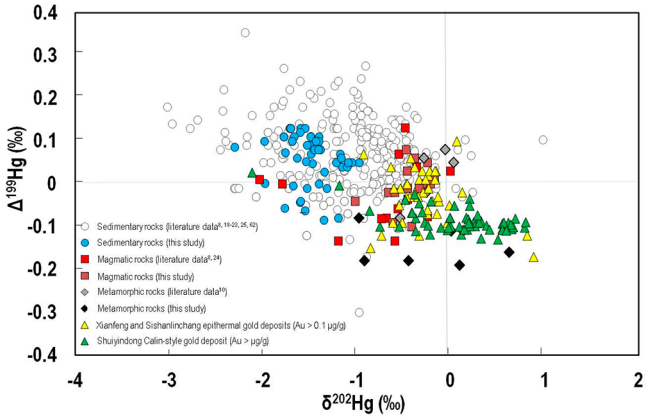

Figure 5. Hg isotopic composition of major rock units, epithermal, and Carlin-type gold deposits studied. The data points for epithermal and Carlin gold deposits are those with Au above 0.1 μg/g. External reproducibility of the analyses is about 0.1 ‰ (2 SD) and 0.04 ‰ (2 SD) for δ^{202}Hg and Δ^{199}Hg, respectively.

the majority of magmatic rocks (δ^{202}Hg: −1 to 0‰; Δ^{199}Hg: −0.1 to 0.1‰) and metamorphic rocks (δ^{202}Hg: −1 to 1‰; Δ^{199}Hg: −0.2 to 0.1‰) have quite different Hg isotope signatures compared to sedimentary rocks (δ^{202}Hg: −3 to 1 ‰; Δ^{199}Hg: −0.6 to 0.4‰).[8,10,18−25,62] The much higher δ^{202}Hg values of igneous and metamorphic rocks may be explained by the fact that magmatism and metamorphism involve thermal processing, which may cause the preferential loss of light Hg isotopes.[7,12] While hydrothermal leaching of Hg from any source rock may cause minor changes in δ^{202}Hg (<±0.5‰, according to Smith et al.[8]), Hg-MIF can be a source tracer of Hg in mineral deposits.[9,10,26] Hg-MIF signals in natural samples have been mainly explained by Hg(II) photoreduction at Earth's surface.[9,15−17] As shown in Figure 5, regarding sedimentary rocks, the negative MIF is mainly due to its high organic matter inherited from terrestrial plants, whereas the positive MIF can be explained by sequestration of residual Hg(II) in aqueous systems.[9,15−17,63] The small or no Hg-MIF in magmatic rocks and metamorphic rocks suggests that Hg in these rocks has been affected by no or very limited photochemical alteration.[8,15] In previous studies, significant Hg-MIF has been observed in Mississippi Valley type (MVT: a variation of ∼0.4‰ for Δ^{199}Hg) and sedimentary exhalative (SEDEX: a variation of ∼0.4‰ for Δ^{199}Hg) Pb−Zn deposits that receive some of their Hg from sedimentary rocks.[9,10,26] Hydrothermal deposits and coal deposits, which have a close relation to magmatic activities, however, showed Δ^{199}Hg of near zero.[9,18,24]

For the Xianfeng and Sishanlinchang deposits, no statistical differences (p > 0.05, t test) in δ^{202}Hg and Δ^{199}Hg can be observed for mineralized rocks$_{Au>0.10}$, indicating they have similar Hg sources. Most rocks$_{Au>0.10}$ in the Xianfeng and Sishanlinchang deposits show insignificant Hg-MIF, which suggests that Hg mainly derives from igneous rocks because these rocks are characterized by the virtual absence of significant Hg-MIF (Δ^{199}Hg: −0.1 to 0.1‰). As mentioned

DOI: 10.1021/acsearthspacechem.9b00111
ACS Earth Space Chem. 2019, 3, 1631−1639

earlier, the two deposits are spatially and temporally associated with igneous rocks. The published $\delta^{34}S$ data (−1.8 to 5‰) from the ore bodies are consistent with a magmatic-hydrothermal (silicate magma) origin for the ore fluid.[47] Only two samples from the Xianfeng deposit showed slightly negative $\Delta^{199}Hg$ values (−0.17‰ and −0.12‰). The leaching of Hg from nearby sedimentary rocks by meteoric or other fluids may explain the Hg-MIF of these two samples.

Interestingly, mineralized $rocks_{Au>0.10}$ from Shuiyindong are isotopically similar to those from Xianfeng and Sishanlinchang (Figure 4), and their composition also differs from sedimentary rocks (Figure 5). The similarities in Hg-MIF signals between the Shuiyindong deposit and the two epithermal deposits suggest that Hg in the Shuiyindong deposit was magmatic rocks, rather than sedimentary rocks. Although igneous and metamorphic rocks are not exposed to any larger extent in the studied area, there are aeromagnetic and gravimetric anomalies that suggest the presence of a larger pluton at about 5 km depth below the Youjiang Basin.[39,42] This is exactly what is observed in the Carlin district where significant Eocence magmatism is vertically connected to Carlin-type gold deposits by pre-existing basemen penetrating faults. Those deposits are hypogene, and it makes perfect sense that the Eocene plutons (magma chambers) were the source of the ore fluids, which also have isotope signatures consistent with a silicate magma source.[4]

It is noteworthy that some barren $rocks_{Au<0.05}$ at the top layer of the Longtan Formation show very negative $\delta^{202}Hg$ of −3 to −4 ‰ (Figure 3). These samples have high Hg concentrations and reflect the Hg enrichment halos around the Shuiyindong deposit. Our data are similar to that of a previous study[7] that observed, in an epithermal system in Nevada, USA, that samples at the top of the system have much lower $\delta^{202}Hg$ than in the underlying veins. This isotopic difference has been ascribed to the boiling of hydrothermal fluids and associated evaporation of isotopically light Hg at the surface of the hydrothermal system.[7] The very negative $\delta^{202}Hg$ values in this study suggest the same mechanism may have occurred at the top layers of the Shuiyindong deposit. A recent fluid-inclusion study observed a decrease of CO_2, CO, and CH_4 from deep layers to top layers of the Shuiyindong deposit, suggesting boiling occurred at later stages when brecciation generated increased permeability at the top layer of the ore system.[64]

CONCLUSIONS

Our reconnaissance study shows that the Hg isotope system is a new tracer to constrain Hg sources in gold deposits based on the example of epithermal and Carlin-type deposits we investigated. By comparing Hg isotopic fingerprints between the studied gold ores and previous results and our new results on magmatic, metamorphic, sedimentary source rocks, this study suggests a plausible origin of magmatic Hg in these gold deposits. Hg in these gold deposits may have come from a silicate magma by mass transfer occurring via an evolved magmatic-hydrothermal fluid. As these deposits are spatially and temporally associated with igneous rocks, magmatism can provide Hg in the ore-forming fluids in the three gold deposits. In the case of the sediment-hosted Shuiyindong Carlin-type gold deposits, our data do not support that Hg would be directly leached from country rocks, but rather favor a magmatic-hydrothermal fluid model as suggested for the classic Carlin gold province in Nevada, USA, where an unexposed pluton is the most likely metal source.[4]

ASSOCIATED CONTENT

Supporting Information

The Supporting Information is available free of charge on the ACS Publications website at DOI: 10.1021/acsearthspacechem.9b00111.

Figures S1 and S2 show the tectonic map of studied areas. Figure S3 shows the mafic and felsic plutons or dikes, the major faults, and the locations. Tables S1 to S3 show the Au and Hg concentrations and Hg isotopic composition of samples from the Xianfeng, Sishanlinchang, and Shuiyindong gold deposits (PDF)

AUTHOR INFORMATION

Corresponding Author

*E-mail: yinrunsheng@mail.gyig.ac.cn.

ORCID

Runsheng Yin: 0000-0001-9631-5303
Ryan F. Lepak: 0000-0003-2806-1895
James P. Hurley: 0000-0003-4430-5319

Notes

The authors declare no competing financial interest.

ACKNOWLEDGMENTS

This work was supported by the Natural Science Foundation of China (41873047). Three anonymous reviewers are acknowledged for their constructive comments that have largely improved the quality of this paper.

REFERENCES

(1) Lindgren, W. A suggestion for the terminology of certain mineral deposits. *Economic Geology* **1922**, *17*, 292−294.

(2) Groves, D. I.; Goldfarb, R. J.; Gebre-Mariam, M.; Hagemann, S. G.; Robert, F. Orogenic gold deposits: A proposed classification in the context of their crustal distribution and relationship to other gold deposit types. *Ore Geol. Rev.* **1998**, *13*, 7−27.

(3) Radtke, A. S.; Rye, R. O.; Dickson, F. W. Geology and stable isotope studies of the Carlin gold deposit, Nevada. *Econ. Geol. Bull. Soc. Econ. Geol.* **1980**, *75*, 641−672.

(4) Muntean, J. L.; Cline, J. S.; Simon, A. C.; Longo, A. A. Magmatic-hydrothermal origin of Nevada's Carlin-type gold deposits. *Nat. Geosci.* **2011**, *4*, 122−127.

(5) Rytuba, J. J. Mercury from mineral deposits and potential environmental impact. *Environ. Geol.* **2003**, *43*, 326−338.

(6) Hedenquist, J. W.; Arribas, A.; Gonzalez-Urien, E. Exploration for epithermal gold deposits. *Reviews in Economic Geology* **2000**, *13*, 45−77.

(7) Smith, C. N.; Kesler, S. E.; Klaue, B.; Blum, J. D. Mercury isotope fractionation in fossil hydrothermal systems. *Geology* **2005**, *33*, 825−828.

(8) Smith, C. N.; Kesler, S. E.; Blum, J. D.; Rytuba, J. J. Isotope geochemistry of mercury in source rocks, mineral deposits and spring deposits of the California Coast Ranges, USA. *Earth Planet. Sci. Lett.* **2008**, *269*, 399−407.

(9) Yin, R.; Feng, X.; Hurley, J. P.; Krabbenhoft, D. P.; Lepak, R. F.; Hu, R.; Zhang, Q.; Li, Z.; Bi, X. Mercury isotopes as proxies to identify sources and environmental impacts of mercury in sphalerites. *Sci. Rep.* **2016**, *6*, 18686.

(10) Xu, C.; Yin, R.; Peng, J.; Hurley, J. P.; Lepak, R. F.; Gao, J. F.; Feng, X.; Hu, R.; Bi, X. Mercury isotope constraints on the source for sediment-hosted lead-zinc deposits in the Changdu area, southwestern China. *Miner. Deposita* **2018**, *53*, 339−352.

(11) Bergquist, B. A.; Blum, J. D. Mass-dependent and-independent fractionation of Hg isotopes by photoreduction in aquatic systems. *Science* **2007**, *318*, 417−420.

DOI: 10.1021/acsearthspacechem.9b00111
ACS Earth Space Chem. 2019, 3, 1631−1639

(12) Estrade, N.; Carignan, J.; Sonke, J. E.; Donard, O. F. Mercury isotope fractionation during liquid-vapor evaporation experiments. *Geochim. Cosmochim. Acta* **2009**, *73*, 2693−2711.
(13) Zheng, W.; Hintelmann, H. Mercury isotope fractionation during photoreduction in natural water is controlled by its Hg/DOC ratio. *Geochim. Cosmochim. Acta* **2009**, *73*, 6704−6715.
(14) Wiederhold, J. G.; Cramer, C. J.; Daniel, K.; Infante, I.; Bourdon, B.; Kretzschmar, R. Equilibrium mercury isotope fractionation between dissolved Hg(II) species and thiol-bound Hg. *Environ. Sci. Technol.* **2010**, *44*, 4191−4197.
(15) Bergquist, B. A.; Blum, J. D. The odds and evens of mercury isotopes: applications of mass-dependent and mass-independent isotope fractionation. *Elements* **2009**, *5*, 353−357.
(16) Sonke, J. E. A global model of mass independent mercury stable isotope fractionation. *Geochim. Cosmochim. Acta* **2011**, *75*, 4577−4590.
(17) Blum, J. D.; Sherman, L. S.; Johnson, M. W. Mercury isotopes in Earth and environmental sciences. *Annu. Rev. Earth Planet. Sci.* **2014**, *42*, 249−269.
(18) Sun, R.; Sonke, J. E.; Liu, G.; Zheng, L.; Wu, D. Variations in the stable isotope composition of mercury in coal-bearing sequences: Indications for its provenance and geochemical processes. *Int. J. Coal Geol.* **2014**, *133*, 13−23.
(19) Thibodeau, A. M.; Ritterbush, K.; Yager, J. A.; West, A. J.; Ibarra, Y.; Bottjer, D. J.; Berelson, W. M.; Bergquist, B. A.; Corsetti, F. A. Mercury anomalies and the timing of biotic recovery following the end-Triassic mass extinction. *Nature Communication* **2016**, *7*, 11147.
(20) Gong, Q.; Wang, X.; Zhao, L.; Grasby, S. E.; Chen, Z. Q.; Zhang, L.; Yang, L.; Cao, L.; Li, Z. Mercury spikes suggest volcanic driver of the Ordovician-Silurian mass extinction. *Sci. Rep.* **2017**, *7*, 5304.
(21) Grasby, S. E.; Shen, W.; Yin, R.; Gleason, J. D.; Blum, J. D.; Lepak, R. F.; Hurley, J. P.; Beauchamp, B. Isotopic signatures of mercury contamination in latest Permian oceans. *Geology* **2017**, *45*, 55−58.
(22) Yin, R.; Xu, L.; Lehmann, B.; Lepak, R. F.; Hurley, J. P.; Mao, J.; Feng, X.; Hu, R. Anomalous mercury enrichment in Early Cambrian black shales of South China: Mercury isotopes indicate a seawater source. *Chem. Geol.* **2017**, *467*, 159−167.
(23) Wang, X.; Cawood, P. A.; Zhao, H.; Zhao, L.; Grasby, S. E.; Chen, Z. Q.; Wignall, P. B.; Lv, Z.; Han, C. Mercury anomalies across the end Permian mass extinction in South China from shallow and deep water depositional environments. *Earth Planet. Sci. Lett.* **2018**, *496*, 159−167.
(24) Zheng, L.; Sun, R.; Hintelmann, H.; Zhu, J.; Wang, R.; Sonke, J. E. Mercury stable isotope compositions in magmatic-affected coal deposits: New insights to mercury sources, migration and enrichment. *Chem. Geol.* **2018**, *479*, 86−101.
(25) Zheng, W.; Gilleaudeau, G. J.; Kah, L. C.; Anbar, A. D. Mercury isotope signatures record photic zone euxinia in the Mesoproterozoic ocean. *Proc. Natl. Acad. Sci. U. S. A.* **2018**, *115*, 10594−10599.
(26) Sonke, J. E.; Schäfer, J.; Chmeleff, J.; Audry, S.; Blanc, G.; Dupré, B. Sedimentary mercury stable isotope records of atmospheric and riverine pollution from two major European heavy metal refineries. *Chem. Geol.* **2010**, *279*, 90−100.
(27) Jasinski, S. M. Mineral commodity summaries 2016. *US Geological Survey* **2016**, 124−125.
(28) Rui-Zhong, H.; Wen-Chao, S.; Xian-Wu, B.; Guang-Zhi, T.; Hofstra, A. Geology and geochemistry of Carlin-type gold deposits in China. *Mineralium Deposita* **2002**, *37*, 378−392.
(29) Peters, S. G.; Huang, J.; Li, Z.; Jing, C. Sedimentary rock-hosted Au deposits of the Dian-Qian-Gui area, Guizhou, and Yunnan Provinces, and Guangxi District, China. *Ore Geology Reviews* **2007**, *31*, 170−204.
(30) Zhang, Z.; Mao, J.; Wang, Y.; Pirajno, F.; Liu, J.; Zhao, Z. Geochemistry and geochronology of the volcanic rocks associated with the Dong'an adularia-sericite epithermal gold deposit, Lesser Hinggan Range, Heilongjiang province, NE China: Constraints on the metallogenesis. *Ore Geol. Rev.* **2010**, *37*, 158−174.
(31) Zhai, D.; Liu, J.; Ripley, E. M.; Wang, J. eochronological and He-Ar-S isotopic constraints on the origin of the Sandaowanzi gold-telluride deposit, northeastern China. *Lithos* **2015**, *212*, 338−352.
(32) Mizutani, S.; Kojima, S. Mesozoic radiolarian biostratigraphy of Japan and collage tectonics along the eastern continental margin of Asia. *Palaeogeogr., Palaeoclimatol., Palaeoecol.* **1992**, *96*, 3−22.
(33) Şengör, A. M. C.; Natal'In, B. A.; Burtman, V. S. Evolution of the Altaid tectonic collage and Palaeozoic crustal growth in Eurasia. *Nature* **1993**, *364*, 299.
(34) Wu, F. Y.; Yang, J. H.; Lo, C. H.; Wilde, S. A.; Sun, D. Y.; Jahn, B. M. The Heilongjiang Group: a Jurassic accretionary complex in the Jiamusi Massif at the western Pacific margin of northeastern China. *Isl. Arc* **2007**, *16*, 156−172.
(35) Li, W.; Liu, Y.; Takasu, A.; Zhao, Y.; Fazle, K. M.; Wen, Q.; Liang, C.; Feng, Z.; Zhang, L. Metamorphic evolution of the Heilongjiang glaucophanic rocks, NE China: Constraints from the P-T pseudosections in the NCKFMASHTO system. *Geological Journal* **2019**, *54*, 698−715.
(36) Wilde, S. A.; Zhang, X.; Wu, F. Extension of a newly identified 500 Ma metamorphic terrane in North East China: further U-Pb SHRIMP dating of the Mashan Complex, Heilongjiang Province, China. *Tectonophysics* **2000**, *328*, 115−130.
(37) Wilde, S. A.; Wu, F.; Zhang, X. Late Pan-African magmatism in northeastern China: SHRIMP U-Pb zircon evidence from granitoids in the Jiamusi Massif. *Precambrian Res.* **2003**, *122*, 311−327.
(38) Sun, M. D.; Xu, Y. G.; Wilde, S. A.; Chen, H. L.; Yang, S. F. The Permian Dongfanghong island-arc gabbro of the Wandashan Orogen, NE China: implications for Paleo-Pacific subduction. *Tectonophysics* **2015**, *659*, 122−136.
(39) Xie, Z.; Xia, Y.; Cline, J. S.; Pribil, M. J.; Koenig, A.; Tan, Q.; Wei, D.; Wang, Z.; Yan, J. Magmatic origin for sediment-hosted Au deposits, Guizhou Province, China: In situ chemistry and sulfur isotope composition of pyrites, Shuiyindong and Jinfeng deposits. *Economic Geology* **2018**, *113*, 1627−1652.
(40) Zhu, J. J.; Hu, R. Z.; Richards, J. P.; Bi, X. W.; Stern, R.; Lu, G. No genetic link between Late Cretaceous felsic dikes and Carlin-type Au deposits in the Youjiang basin, Southwest China. *Ore Geol. Rev.* **2017**, *84*, 328−337.
(41) Tan, Q. P.; Xia, Y.; Xie, Z. J.; Yan, J. Migration paths and precipitation mechanisms of ore-forming fluids at the Shuiyindong Carlin-type gold deposit, Guizhou, China. *Ore Geol. Rev.* **2015**, *69*, 140−156.
(42) Su, W.; Dong, W.; Zhang, X.; Shen, N.; Hu, R.; Hofstra, A. H.; Cheng, L.; Xia, Y.; Yang, K. Carlin-type gold deposits in the Dian-Qian-Gui "Golden Triangle" of Southwest China. *Reviews in Economic Geology* **2018**, *19*, 157−186.
(43) Wang, Q. Geological characteristics and genesis of the Xianfengbeishan gold deposit in Wandashan Area, Heilongjiang Province. Jilin University Master Thesis 2015. (in Chinese with English abstract).
(44) Yang, J.; Quan, C.; Liu, X. The alteration characteristics and genesis analysis of Xianfeng north mountain gold mine in Heilongjiang Province. *Gold Science and Technology* **2005**, *13*, 26−29 (in Chinese with English abstract) .
(45) Sun, R.; Quan, C. The alteration and characteristics of the gold deposit at the north peak of Xianfeng Mountain, Hulin City, Heilongjiang Province. *Gold* **2006**, *24*, 11−15 (in Chinese with English abstract) .
(46) Guo, J. *Study on ore genesis and geological characteristics of Sishan gold deposit, Heilongjiang province*. Jilin University Master Thesis 2012 (In Chinese with English abstract).
(47) Huang, Y.; Liu, J.; Gao, C. Geochemistry and metallogenic age of Sishanlinchang gold-silver deposit in Jidong of Heilongjiang. *Global Geology* **2011**, *14*, 29−43.
(48) Su, W.; Heinrich, C. A.; Pettke, T.; Zhang, X.; Hu, R.; Xia, B. Sediment-hosted gold deposits in Guizhou, China: products of wall-rock sulfidation by deep crustal fluids. *Econ. Geol. Bull. Soc. Econ. Geol.* **2009**, *104*, 73−93.

DOI: 10.1021/acsearthspacechem.9b00111
ACS Earth Space Chem. 2019, 3, 1631−1639

(49) Su, W. C.; Xia, B.; Zhang, H. T.; Zhang, X. C.; Hu, R. Z. Visible gold in arsenian pyrite at the Shuiyindong Carlin-type gold deposit, Guizhou, China: Implications for the environment and processes of ore formation. *Ore Geol. Rev.* **2008**, *33*, 667−679.
(50) Yin, R.; Krabbenhoft, D. P.; Bergquist, B. A.; Zheng, W.; Lepak, R. F.; Hurley, J. P. Effects of mercury and thallium concentrations on high precision determination of mercury isotopic composition by Neptune Plus multiple collector inductively coupled plasma mass spectrometry. *J. Anal. At. Spectrom.* **2016**, *31*, 2060−2068.
(51) Blum, J. D.; Bergquist, B. A. Reporting of variations in the natural isotopic composition of mercury. *Anal. Bioanal. Chem.* **2007**, *388*, 353−359.
(52) Donovan, P. M.; Blum, J. D.; Yee, D.; Gehrke, G.; Singer, M. B. An isotopic record of mercury in San Francisco Bay sediment. *Chem. Geol.* **2013**, *349*, 87−98.
(53) Li, J. Sulfur isotopes and trace elements constraints on the formation and evolution of the Carlin-type gold deposits in SW China. University of Chinese Academy of Sciences Ph.D. Thesis, 2019 (in Chinese with English abstract).
(54) Zhu, Y.; An, F.; Tan, J. Geochemistry of hydrothermal gold deposits: a review. *Geosci. Front.* **2011**, *2*, 367−374.
(55) Saunders, J. A.; Hofstra, A. H.; Goldfarb, R. J.; Reed, M. H. Geochemistry of hydrothermal gold deposits. In *Treatise on Geochemistry*, 2nd ed.; Holland, H. D., Turekian, K. K., Eds.; Elsevier: Oxford, UK, 2014; Vol. *13*, pp 383−424.
(56) Sillitoe, R. H.; Hedenquist, J. W. Linkages between volcanotectonic settings, ore-fluid compositions, and epithermal precious metal deposits. *Special Publication-Society of Economic Geologists* **2003**, *10*, 315−343.
(57) Sun, W. D.; Ding, X.; Hu, Y.-H.; Li, X.-H. The golden transformation of the Cretaceous plate subduction in the west Pacific. *Earth Planet. Sci. Lett.* **2007**, *262*, 533−542.
(58) Ohmoto, H. Systematics of sulfur and carbon isotopes in hydrothermal ore deposits. *Econ. Geol. Bull. Soc. Econ. Geol.* **1972**, *67*, 551−578.
(59) Rye, R. O.; Ohmoto, H. Sulfur and carbon isotopes and ore genesis: a review. *Econ. Geol. Bull. Soc. Econ. Geol.* **1974**, *69*, 826−842.
(60) Simmons, S. F.; White, N.; John, D. A. Geological characteristics of epithermal precious and base metal deposits. *Economic Geology One Hundredth Anniversary* **2005**, 485−522.
(61) Sherman, L. S.; Blum, J. D.; Nordstrom, D. K.; McCleskey, R. B.; Barkay, T.; Vetriani, C. Mercury isotopic composition of hydrothermal systems in the Yellowstone Plateau volcanic field and Guaymas Basin sea-floor rift. *Earth Planet. Sci. Lett.* **2009**, *279*, 86−96.
(62) Shen, J.; Chen, J.; Algeo, T. J.; Yuan, S.; Feng, Q.; Yu, J.; Zhou, L.; O'Connell, B.; Planavsky, N. J. Evidence for a prolonged Permian-Triassic extinction interval from global marine mercury records. *Nat. Commun.* **2019**, *10*, 1563.
(63) Sun, R.; Jiskra, M.; Amos, H. M.; Zhang, Y.; Sunderland, E. M.; Sonke, J. E. Modelling the mercury stable isotope distribution of Earth surface reservoirs: Implications for global Hg cycling. *Geochim. Cosmochim. Acta* **2019**, *246*, 156−173.
(64) Wu, S. Y.; Hou, L.; Ding, J.; Wu, W.; Qin, K.; Zhang, J. R.; Zhu, S. B. Ore-controlling structure types and characteristics of ore-forming fluid of the Carlin-type gold orefield in southwestern Guizhou, China. *Acta Petrologica Sinica* **2016**, *32*, 2407−2424 (in Chinese with English abstract) .

DOI: 10.1021/acsearthspacechem.9b00111
ACS Earth Space Chem. 2019, 3, 1631−1639